AVERAGE INPUT CURRENT MODE CONTROL OF TWO-PHASE INTERLEAVED BOOST CONVERTER USING LOW-COST MICROCONTROLLER

YIN YIN PHYO[1], TUN LIN NAING[2]
Power Electronic, Drives and Control Research Team
Department of Electrical Power Engineering
Mandalay Technological University
Mandalay, Myanmar

[1]yinyinphyo2000@gmail.com, [2]tunlinnaing1980@gmail.com

Abstract*—In this paper, the average input current mode control is proposed for two-phase interleaved boost converter with two separate input inductors operating in continuous conduction mode (CCM). The required mathematical model is obtained from the equivalent circuits of its different four modes of operation. The small ripple approximation is derived to find the transfer functions from dynamic model using switching function. In average input current mode control, the inner current loop and outer voltage loop are designed with PI controller using bode analysis. Anti-windup structure is applied for PI controllers in control system. Moreover, the simulation work has been studied by using mathematical models. And, the hardware prototype is implemented by using low-cost microcontroller Arduino Nano. Finally, the laboratory prototype, available from the local market, is constructed to validate the mathematical model. The results show that the output voltage response is the faster rise time and settling time with acceptable overshoot.*

Keywords*- Average input current mode control- Interleaved boost converter- Low-cost microcontroller-PI controller- Switching function.*

I. INTRODUCTION

In recent years, DC-DC converters are widely used in many applications such as DC drives, computer power supply, renewable energy source and automotive, power factor correction and so on [1-3]. But, the conventional boost converter has many disadvantages such as the large output capacitor is required to reduce the ripple voltage, larger input current ripple and poor efficiency. Interleaved topology is used to solve this problem.

There are many methods to analyze the converters. Subrata Banerjee [4] presented the two-phase IBC without considering all parasitic elements to find the transfer function from the state-space averaging technique. But, the state-space averaging method is sometimes complex when the converter circuit contains many elements. Therefore, the signal flow graph (SFG) nonlinear graphical modeling method was developed for PWM converter to solve the above problem in [5]. But, these methods are complex and many mathematical equations are needed.

The IBC has right-half plane zero (RHPZ) in output voltage to control transfer function. But, transfer functions of inductor current for two-phase IBC do not have the RHPZ. RHPZ can cause slow and undershoot the system response. The input current is high during starting although the output voltage is regulated in voltage mode control [6]. Therefore, the current mode method is important in order to avoid these effects. There are many current mode control methods such as average current mode control, peak current control and slope current control. Among them, average current mode control method is proposed in this paper because this method is easily to compensate the system.

BUPT

Fellipe S [7] studied the six-phase interleaved double dual boost converter and the output is controlled using current mode control. The output of voltage controller is used as the reference of current loop (internal loop). Sandeep Kolluri [8] presented the average current mode control using independent current loops and load voltage is regulated using output voltage loop for two-phase IBC and constructed the average current mode controller card. Hung-Chi Chen [9] proposed decoupled current-balancing control (DCBC) with the voltage-regulating loop and current balancing loop are parallel for two-phase IBC.

Two current sensors are required to implement current balancing function for two-phase IBC [10-12]. The current sensing is an important function for current control of converter. Some papers are proposed several circuit topologies and control schemes to reduce the number of current sensors [8,13].

Moreover, many control methods are proposed in [14-18], such as voltage mode control, current mode control, sliding mode control, predictive control, one-cycle control and so on. These proposed control methods are used to improve the voltage regulation. The controller design of these methods are more complicated although their performance is good.

The first objective of this paper is to derive the transfer function from small-signal analysis using dynamic model with switching function. This approach, is distinct from other methods [4,5]. This method is easier to achieve the transfer function with minimum mathematical equations.

The second objective is to implement the average input current mode control of two-phase IBC using low-cost microcontroller. In this regard, this paper proposes the low-cost microcontroller Arduino Nano. There are many reasons for using it. Firstly, it is small, cheap and compact. Secondly, the use of a software programming and hardware implementation is easily understood and friendly than the other microcontrollers for the users. Thirdly, it can be easily obtained from the market in Myanmar. In recent years, Arduino is widely used as a compensator for converter control [19,20].

The remaining sections of this paper are described as follows. The mathematical modeling of two-phase IBC is described in section 2. The PI controller gains for inner current loop and outer voltage loop are calculated in section 3. Simulation and experimental results are discussed in section 4 and 5. Finally, this paper is concluded in section 6.

II. MATHEMATICAL MODELING OF TWO-PHASE INTERLEAVED BOOST CONVERTER

The two-phase interleaved boost converter with control scheme is illustrated in Fig. 1. The two-phase IBC consists of separate input inductors L_1 and L_2, Switches S_1 and S_2, Diodes D_1 and D_2 and the same filter capacitor C at the output. The switches S_1 and S_2 have the same switching frequency. The load is represented by a resistor R. The inductor stored and released energy when the switch is ON and OFF. The capacitor is used for filtering the ripple in the output voltage V_o. The gate signals of switches S_1 and S_2 are represented by u_1 and u_2. The possible values of gate switches are $u_1 \in \{0,1\}$ and $u_2 \in \{0,1\}$, in which 0 and 1 represent OFF and ON states of the power switches. And, the gate signal of switches u_1 and u_2 are applied 180 degree phase shift.

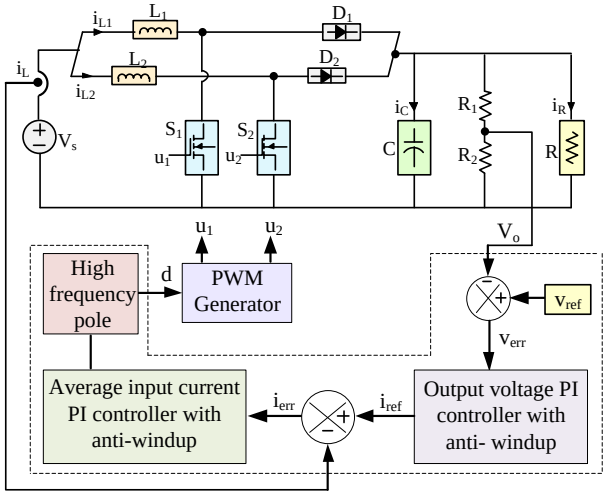


Fig. 1. Circuit diagram of two-phase IBC with control scheme

BUPT

In proposed control scheme, outer voltage loop and inner current loop are contained. PI controller with anti-windup is designed for both control loops. The input voltage range of microcontroller is 0-5V. Therefore, it is needed to reduce the converter output voltage. R_1 and R_2 are applied to solve the above problem by using the voltage divider method. It helps to send the converter output voltage to the microcontroller. The outer loop is generated the reference current (i_{ref}) and the inner loop is generated the duty cycle (d), respectively. This duty cycle is used to generate the PWM signal. These PWM signals are fed into the gates of switches u_1 and u_2.

A. Switched-Function Model

The system has four logics because the gate signals of u_1 and u_2 have two states (i.e. 0 and 1). Therefore, the system are operated in four modes. The inductor resistance is considered in this paper but the parasitic elements such as MOSFET ON resistance, diode voltage drop and capacitor parasitic resistance are not considered. The converter is assumed as operate in continuous conduction mode (CCM). Also, it can be assumed that the value of inductors are the same $L_1=L_2=L$ for converter operation can easily be done. The equivalent circuits of four modes are shown as the following figures.

Mode 1: $u_1=1$ and $u_2=0$. Fig. 2 illustrates the equivalent circuit of mode 1.

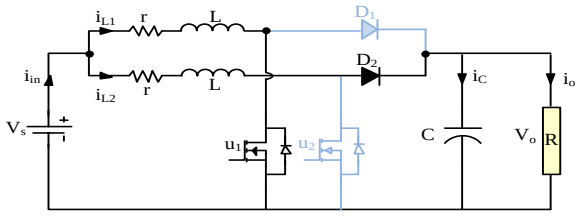


Fig. 2. Equivalent circuit for Mode 1

For equivalent circuit of Mode 1, the following differential equations are obtained by applying *Kirchhoff's voltage and current laws.*

$$L\frac{di_{L1}}{dt}=V_s-ri_{L1} \quad (1)$$

$$L\frac{di_{L2}}{dt}=V_s-ri_{L2}-v_o \quad (2)$$

$$C\frac{dv_o}{dt}=i_{L2}-\frac{v_o}{R} \quad (3)$$

Mode 2: $u_1=0$ and $u_2=1$. Fig. 3 shows the equivalent circuit of mode 2.

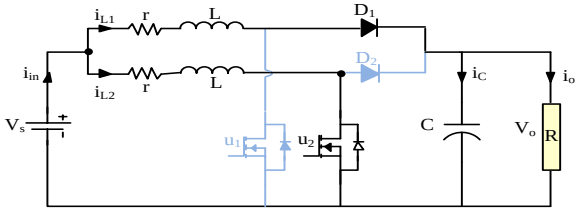


Fig. 3. Equivalent circuit for Mode 2

For equivalent circuit of Mode 2, the following differential equations are obtained by applying *Kirchhoff's voltage and current laws.*

$$L\frac{di_{L1}}{dt}=V_s-ri_{L1}-v_o \quad (4)$$

$$L\frac{di_{L2}}{dt}=V_s-ri_{L2} \quad (5)$$

$$C\frac{dv_o}{dt}=i_{L1}-\frac{v_o}{R} \quad (6)$$

Mode 3: $u_1=u_2=1$. Fig. 4 illustrates the equivalent circuit of mode 3.

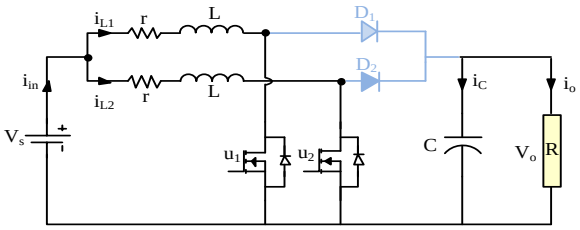


Fig. 4. Equivalent circuit for Mode 3

For equivalent circuit of Mode 3, the following differential equations are obtained by applying *Kirchhoff's voltage and current laws.*

$$L\frac{di_{L1}}{dt}=V_s-ri_{L1} \quad (7)$$

$$L\frac{di_{L2}}{dt}=V_s-ri_{L2} \quad (8)$$

$$C\frac{dv_o}{dt}=-\frac{v_o}{R} \quad (9)$$

BUPT

Mode 4: $u_1=u_2=0$. Fig. 5 shows the equivalent circuit of mode 4.

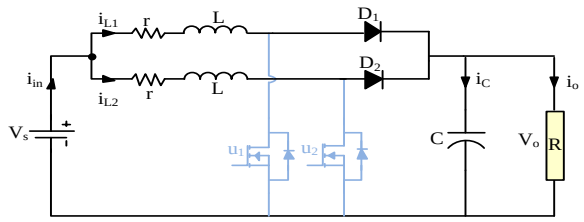


Fig. 5. Equivalent circuit for Mode 4

For equivalent circuit of Mode 4, the following differential equations are obtained by applying *Kirchhoff's voltage and current laws.*

$$L\frac{di_{L1}}{dt}=V_s-ri_{L1}-v_o \tag{10}$$

$$L\frac{di_{L2}}{dt}=V_s-ri_{L2}-v_o \tag{11}$$

$$C\frac{dv_o}{dt}=i_{L1}+i_{L2}-\frac{v_o}{R} \tag{12}$$

The following differential equations are presented by using switched-function.

$$L\frac{di_{L1}}{dt}=V_s-ri_{L1}-(1-u_1)v_o \tag{13}$$

$$L\frac{di_{L2}}{dt}=V_s-ri_{L2}-(1-u_2)v_o \tag{14}$$

$$C\frac{dv_o}{dt}=(1-u_1)i_{L1}+(1-u_2)i_{L2}-\frac{v_o}{R} \tag{15}$$

B. *Steady-state Equations of the System*

The average model of the system is used to obtain the steady-state equations. The average positions d_1 and d_2 replace the switch positions u_1 and u_2 in (13)-(15).

$$L\frac{d\bar{i}_{L1}}{dt}=V_s-r\bar{i}_{L1}-(1-d_1)\bar{v}_o \tag{16}$$

$$L\frac{d\bar{i}_{L2}}{dt}=V_s-r\bar{i}_{L2}-(1-d_2)\bar{v}_o \tag{17}$$

$$C\frac{d\bar{v}_o}{dt}=(1-d_1)\bar{i}_{L1}+(1-d_2)\bar{i}_{L2}-\frac{\bar{v}_o}{R} \tag{18}$$

whereas, $\bar{u}_1=d_1\in[0,1]$ and $\bar{u}_2=d_2\in[0,1]$ are the average positions of the switches. The values of d_1 and d_2 are the addition of average and small signal value.

$$d_1=D_1+\tilde{d}_1 \text{ and } d_2=D_2+\tilde{d}_2 \tag{19}$$

If $\tilde{d}\ll D$, $\tilde{d}$ is neglected by using small-signal approximation. d_1 and d_2 are equal to D in steady-state condition. Therefore, $d_1=d_2=D$.

$$0=V_s-rI_{L1}-(1-D)V_o \tag{20}$$

$$0=V_s-rI_{L2}-(1-D)V_o \tag{21}$$

$$0=(1-D)I_{L1}+(1-D)I_{L2}-\frac{V_o}{R} \tag{22}$$

In matrix form, (20)-(22) can be represented as the follow.

$$\begin{pmatrix} r & 0 & (1-D) \\ 0 & r & (1-D) \\ (1-D) & (1-D) & -\frac{1}{R} \end{pmatrix}\begin{pmatrix} I_{L1} \\ I_{L2} \\ V_o \end{pmatrix}=\begin{pmatrix} V_s \\ V_s \\ 0 \end{pmatrix} \tag{23}$$

Equation (24) is derived by using (23) and it represents the steady-state condition of the system.

$$\begin{pmatrix} I_{L1} \\ I_{L2} \\ V_o \end{pmatrix}=\begin{pmatrix} \frac{1}{2R(1-D)^2+r} \\ \frac{1}{2R(1-D)^2+r} \\ \frac{2R(1-D)}{2R(1-D)^2+r} \end{pmatrix}V_s \tag{24}$$

C. *Small-signal Transfer Function*

The average model is used to find the transfer function from small-signal analysis. The average value of this system is the addition of large-signal and small-signal value.

$$\frac{d(I_{L1}+\tilde{i}_{L1})}{dt}=\begin{pmatrix} \frac{V_s-rI_{L1}-r\tilde{i}_{L1}-V_o-\tilde{v}_o}{L} \\ +\frac{DV_o+D\tilde{v}_o+\tilde{d}V_o+\tilde{d}\tilde{v}_o}{L} \end{pmatrix} \tag{25}$$

BUPT

$$\frac{d(I_{L2}+\tilde{i}_{L2})}{dt}=\left(\begin{array}{l}\dfrac{V_s-rI_{L2}-r\tilde{i}_{L2}-V_o-\tilde{v}_o}{L}\\ +\dfrac{DV_o+D\tilde{v}_o+\tilde{d}V_o+\tilde{d}\tilde{v}_o}{L}\end{array}\right) \quad (26)$$

$$\frac{d(V_o+\tilde{v}_o)}{dt}=\left(\begin{array}{l}\dfrac{I_{L1}+\tilde{i}_{L1}-DI_{L1}-D\tilde{i}_{L1}-\tilde{d}I_{L1}-\tilde{d}\tilde{i}_{L1}}{C}\\ +\dfrac{I_{L2}+\tilde{i}_{L2}-DI_{L2}-D\tilde{i}_{L2}-\tilde{d}I_{L2}-\tilde{d}\tilde{i}_{L2}-\dfrac{V_o}{R}-\dfrac{\tilde{v}_o}{R}}{C}\end{array}\right) \quad (27)$$

Neglect the non-linear and steady-state terms for the small-signal analysis in (25)-(27). In matrix form, the small-signal model can be represented as follow.

$$\begin{bmatrix}\dfrac{d\tilde{i}_{L1}}{dt}\\ \dfrac{d\tilde{i}_{L2}}{dt}\\ \dfrac{d\tilde{v}_o}{dt}\end{bmatrix}=\begin{bmatrix}-\dfrac{r}{L} & 0 & -\dfrac{D'}{L}\\ 0 & -\dfrac{r}{L} & -\dfrac{D'}{L}\\ \dfrac{D'}{C} & \dfrac{D'}{C} & -\dfrac{1}{RC}\end{bmatrix}\begin{bmatrix}\tilde{i}_{L1}\\ \tilde{i}_{L2}\\ \tilde{v}_o\end{bmatrix}+\begin{bmatrix}\dfrac{V_o}{L}\\ \dfrac{V_o}{L}\\ -\dfrac{(I_{L1}+I_{L2})}{C}\end{bmatrix}\tilde{d}+\begin{bmatrix}\dfrac{1}{L}\\ \dfrac{1}{L}\\ 0\end{bmatrix}V_s \quad (28)$$

The steady-state value of output voltage (V_o) and inductors current (I_{L1},I_{L2}) from (24) are substituted in (28). The transfer functions of two-phase IBC is obtained from (28) by using Laplace transform. Equation (29) is the transfer functions of two-phase IBC.

$$\begin{bmatrix}\tilde{i}_{L1}(s)\\ \tilde{i}_{L2}(s)\\ \tilde{v}_o(s)\end{bmatrix}=\begin{bmatrix}\dfrac{(2D'RV_s)(RCs+2)}{(2D'^2R+r)(r+Ls+2D'^2R+RLCs^2+RCrs)}\\ \dfrac{(2D'RV_s)(RCs+2)}{(2D'^2R+r)(r+Ls+2D'^2R+RLCs^2+RCrs)}\\ \dfrac{-(2RV_s)(-2D'^2R+r+Ls)}{(2D'^2R+r)(r+Ls+2D'^2R+RLCs^2+RCrs)}\end{bmatrix}\tilde{d}(s) \quad (29)$$

III. Controller Design

The input of the voltage controller is the error between the comparison of reference voltage (V_{ref}) and converter's output voltage (V_o) as shown in Fig. 1. The voltage controller generates the average input current reference (i_{ref}) and the current controller determines the duty cycle (d) value. The converter's parameters are shown in Table I. The desired output voltage (reference voltage) is defined 24V. Fig. 6 illustrates the closed-loop control diagram for two-phase IBC.

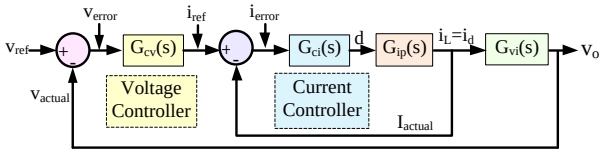


Fig. 6. Closed-loop control system of two-phase IBC

TABLE I

CONVERTER PARAMETERS

Parameters	Variables	Values	Unit
Supply voltage	V_s	12	V
Output voltage	V_o	24	V
Inductors	L_1,L_2	2	mH
Inductor resistance	r	0.2	Ω
Capacitor	C	470	μF
Load Power	P_o	32	W
Load resistance	R	18	Ω
Duty cycle	D	50	%
Switching frequency	f_s	4	kHz

A. Controller Design for Average Current Loop

Fig. 7 shows the block diagram of average input current loop with PI controller. The high frequency pole is included in current controller.

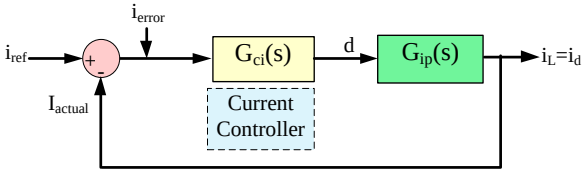


Fig. 7. Block diagram for average current loop control

Control to average current transfer function is calculated from (29) by using converter's parameters of Table I.

BUPT

$$G_{ip}(s)=\frac{\tilde{i}_L(s)}{\tilde{d}(s)}=\frac{\frac{\tilde{i}_{L1}(s)}{\tilde{d}(s)}+\frac{\tilde{i}_{L2}(s)}{\tilde{d}(s)}}{2}$$

$$G_{ip}(s)=\frac{1.827s+432}{0.0001557s^2+0.03397s+84.64} \quad (30)$$

Equation (30) can be represented as follow in (31). This equation is obtained from [21].

$$G_{ip}(s)=G_{ip0}\times\frac{1+\frac{s}{\omega_z}}{1+\frac{s}{\omega_0 Q}+\frac{s^2}{\omega_0^{\ 2}}} \quad (31)$$

Where ω_z is the zero frequency, ω_0 is the resonant frequency and Q is the quality factor. The uncompensated current loop gain $G_{ip}(s)$ is equal $T_u(s)$. Therefore,

$$T_u(s)=G_{ip}(s) \quad (32)$$

The bode diagram of control to average input current transfer function is shown in Fig. 8. In bode diagram, the gain margin (G_m) is infinity and phase margin (P_m) 90 degree. The zero dB crossed frequency is called the cut off frequency (f_c). The cut off frequency of uncompensated control to output voltage transfer function has 2kHz.

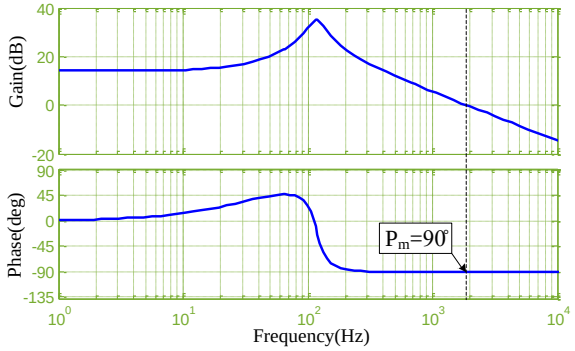


Fig. 8. Bode diagram of uncompensated control to average input current transfer function

The current controller is chosen as a proportional integral (PI) controller. The simple PI compensation law is shown in (33).

$$G_{PI}(s)=G_{PI}(\infty)\left[1+\frac{\omega_{PI}}{s}\right] \quad (33)$$

A high frequency pole is included in compensated transfer function to remove the harmonic content from the switching frequency. The value of high-frequency pole (ω_{HF}) is half of the switching frequency(f_s), that is, at 12566rad/s. The transfer function of controller is described in (34).

$$G_{ci}(s)=G_{PI}(\infty)\left[1+\frac{\omega_{PI}}{s}\right]\times\frac{1}{1+\frac{s}{\omega_{HF}}} \quad (34)$$

The sampling time is defined as 2ms. In order to calculate the controller gains, cut off frequency (f_c) is equal to the sampling frequency as 500Hz. The desired phase margin is defined 70 degree at cut off frequency 500Hz. The phase lag is added to get the desired phase margin. The phase leg is obtained from (35).

$$tan^{-1}\left(\frac{f_c}{f_{HF}}\right)=tan^{-1}\left(\frac{500}{2000}\right)\approx 14^\circ \quad (35)$$

$$\rho'_m=70^\circ+14^\circ=84^\circ$$

The magnitude and phase of the system uncompensated loop gain are calculated at the target cut off frequency.

$$T_u(j\omega_c)\approx 3.953\Rightarrow 11.9dB$$

$$T_u(j\omega_c)\approx -90^\circ \quad (36)$$

The unknown PI coefficients $G_{PI}(\infty)$ and ω_{PI} are calculated as follows. The value of ω_{PI} is derived based on the required phase margin as shown in (37).

$$-\frac{\pi}{2}+tan^{-1}\left(\frac{\omega_c}{\omega_{PI}}\right)+\angle T_u(j\omega_c)=-\pi+\rho'_m \quad (37)$$

And, the value of $G_{PI}(\infty)$ is imposed by the desired cut off frequency in (38).

$$G_{PI}(\infty)\times\sqrt{1+\left(\frac{\omega_c}{\omega_{PI}}\right)^2}\times|T_u(j\omega_c)|=\frac{\omega_c}{\omega_{PI}} \quad (38)$$

BUPT

According to the above equations, the value of $G_{PI}(\infty)$ and ω_{PI} are 0.252 and 330.25rad/s. The values of $G_{PI}(\infty)$ and ω_{PI} are substituted in (33).

$$G_{PI}(s) = 0.252\left[1 + \frac{330.25}{s}\right] \tag{39}$$

If $G_{PI}(s)$ is transformed into $(k_{pi}+k_{ii}/s)$, the resulting k_{pi} is found 0.252 and k_{ii} is found 83.233. The compensated control to average input current transfer function is shown in Fig. 9. In bode diagram, the desired phase margin (P_m) is obtained by using these gains. The value of $G_{PI}(\infty)$, ω_{PI} and ω_{HF} are substituted in (34). The compensator transfer function is

$$G_{ci}(s) = \frac{3167s + 1.05\times10^{6}}{s^{2} + 12566s} \tag{40}$$

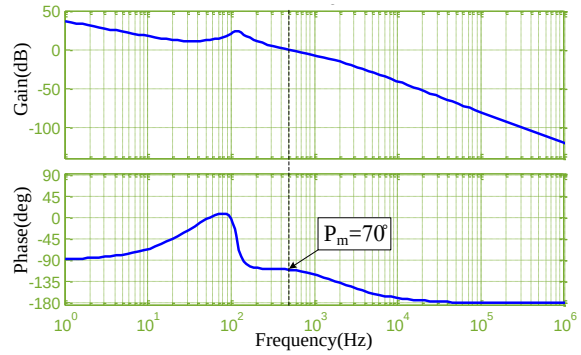


Fig. 9. Bode diagram of compensated open-loop control to average input current transfer function

B. *Controller Design for Voltage Loop*

The closed-loop control diagram of two-phase IBC for total system is illustrated in Fig. 10.

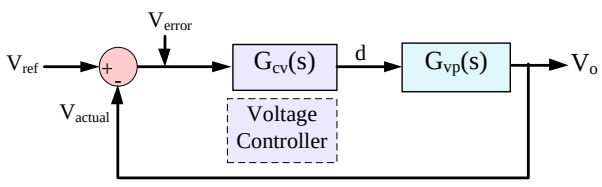


Fig. 10. Block diagram for voltage loop control

The system transfer function $(\tilde{v}_o(s)/\tilde{i}_{ref}(s))$ with average current loop and voltage to diode transfer function is derived as shown in (41).

$$G_{vp}(s) = \frac{\tilde{v}_o(s)}{\tilde{i}_{ref}(s)} = \frac{\tilde{v}_o(s)}{\tilde{i}_d(s)} \times \frac{\tilde{i}_L(s)}{\tilde{i}_{ref}(s)} \tag{41}$$

The voltage to diode transfer function is

$$G_{vi}(s) = \frac{\tilde{v}_o(s)}{\tilde{i}_d(s)} = \frac{R}{1 + RCs} \tag{42}$$

And, $(\tilde{i}_L(s)/\tilde{i}_{ref}(s))$ is obtained from the closed-loop transfer function of inner average current loop.

The bode plot of output voltage to average current reference transfer function is shown in Fig. 11. In bode diagram, the gain margin (G_m) is found 14.5dB and phase margin (P_m) is found 56.5 degree. The cut off frequency of uncompensated output voltage to average current reference transfer function has 300Hz.

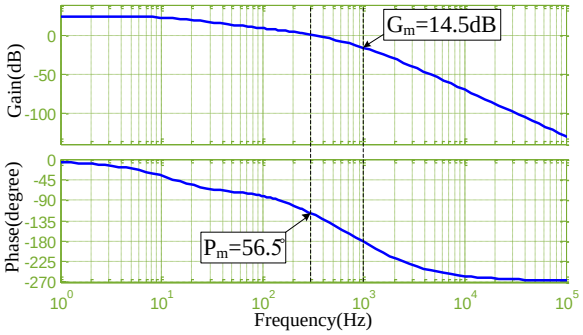


Fig. 11.Bode diagram of uncompensated output voltage to average current reference transfer function

The voltage controller is chosen as a simple proportional integral controller. The PI compensation law is obtained from Gokhan Altintas, et al. (2016) and described in (43).

$$G_{cv}(s) = G(\infty)\left(1 + \frac{\omega_L}{s}\right) \tag{43}$$

Cut off frequency is chosen 20% of sampling frequency as 100Hz. Line frequency is taken 50% of the cut off frequency as 50Hz and ω_L is calculated

BUPT

as 314.16rad/s. According to Fig 7, gain at 100Hz is 9.6dB. G(∞) is calculated as 0.3311 from the following equation.

$$20\log G(\infty) = -9.6dB$$

G(∞) and ω_L is substituted in (43).

$$G_{cv}(s) = 0.3311 + \frac{104.02}{s} \qquad (44)$$

If $G_{cv}(s)$ is transformed into ($k_{pv}+k_{iv}/s$) format, the resulting k_{pv} and k_{iv} are found 0.3311 and 104.02. The compensated transfer function is shown in Fig. 12. The system of magnitude and phase are 23.1dB and 73.6 degree in bode diagram.

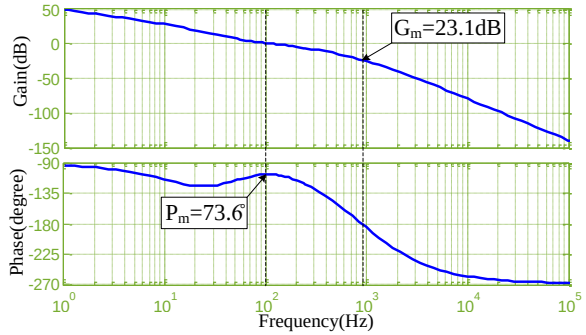


Fig. 12. Compensated open-loop output voltage to average current reference transfer function

The value of controller gains are described in Table II for current and voltage loop.

TABLE II

CONTROLLER GAINS VALUE

Controller Gains	Values
Current proportional gain, k_{pi}	0.252
Current integral gain, k_{ii}	83.223
Voltage proportional gain, k_{pv}	0.3311
Voltage integral gain, k_{iv}	104.02

Fig. 13 is shown the bode diagram of choosing the controller gain based on the sampling frequency. The sample time is very important for the microcontroller. In bode diagram, the system response is slow and more oscillatory when the cut off frequency is less than the sampling frequency. Because higher cut off frequency means higher bandwidth which causes the faster rise time. Therefore, the cut off frequency is chosen equal to the sampling frequency as 500Hz in this paper.

Fig. 14 illustrates the bode diagram of overall open-loop transfer function of two-phase IBC with various load. The value of controller gains are used from Table II. The increasing of the load can cause slow and damp the system response according to Fig. 14. When the load is decreased, the system response is faster rise time. But, it causes more overshoot the system response. Therefore, the rated load resistance is defined 18Ω to find the controller gains.

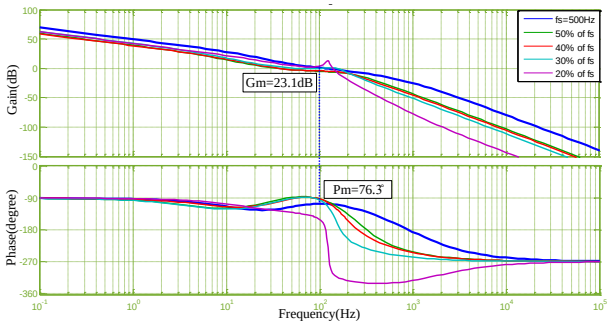


Fig. 13. Bode diagram of choosing the controller gain based on the sample frequency

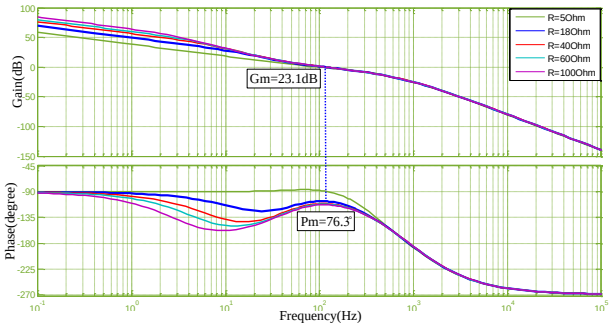


Fig. 14. Bode diagram for compensated overall open-loop transfer function with various load

These controller gains are applied for simulation and experiment using anti-windup. The PI controller with anti-windup structure is shown in Fig. 15.

BUPT

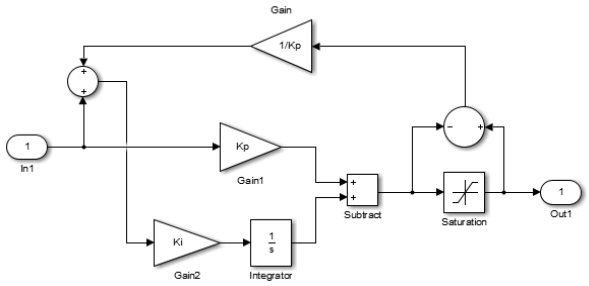
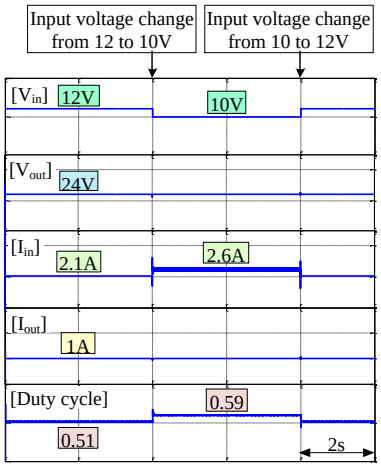


Fig. 15. Simulink blocks of anti-windup structure

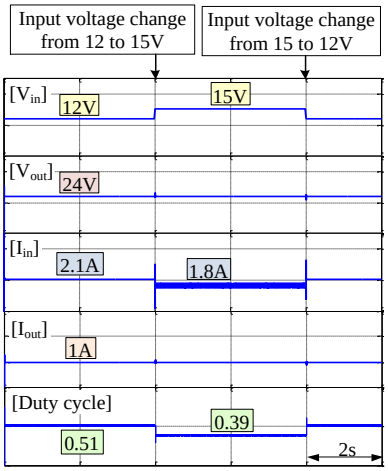
There are many several methods for anti-windup control. Among them, back calculation method is used in this paper. In a common PI controller consists of a proportion part and an integration part. Therefore, anti-windup control is used to prevent integration part from going too high and instability. The system response achieves better transient performance using PI controller with anti-windup control compare to without anti-windup control for converter [11].

IV. Simulation Results

The construction of power converter design consumes more time and cost. Simulation study has done to predict the dynamic performances of the system before actual test. The simulation work is carried out by using Matlab/Simulink. The simulated transient waveforms of two-phase IBC with input voltage change are shown in Fig. 16 for closed-loop control. The load resistance 24Ω is defined for input voltage changes. The simulation running time is defined as 10s.



(a)



(b)

Fig. 16. Simulated transient waveforms of two-phase IBC with input voltage change from (a) 12 to 10 to 12V and (b) 12 to 15 to 12V

Fig. 17 presents the simulated transient waveforms of two-phase IBC with load change for closed-loop test.

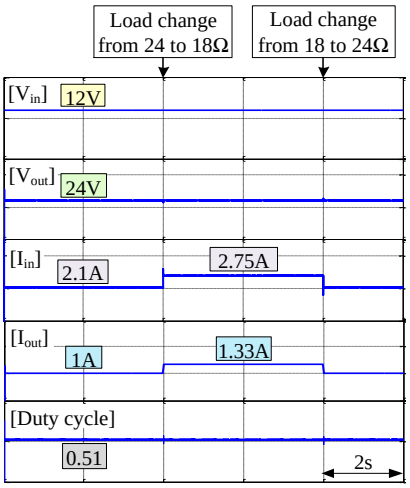


Fig. 17. Simulated transient waveforms of two-phase IBC with load change from 24 to 18 to 24Ω

The start-up response of output voltage is reached the steady-state condition at 0.1s and is found a little overshoot about 8.33%. The output voltage (V_{out}) is suddenly changed during disturbances but it is immediately reached to its set point. When the system is occurred any changes, the

BUPT

input current (I_{in}) is changed as follow as the system changes.

The magnitude of load current (I_{out}) is constant although the magnitude of input voltage (V_{in}) is changed. But, it is varied when the magnitude of load is increased or decreased. The value of duty cycle is changed depend on the situation of input voltage. And, the value of duty cycle is not appreciable change in load perturbation conditions.

When the finding controller gains from section 3 are inserted to the dynamic simulation to test the system, it is tolerance the disturbances such as input voltage change and load change. The start-up response is good because it's rise time has 0.1s. Therefore, these controller gains are continuously used to apply in practical as described in section 5.

V. EXPERIMENT RESULTS

The proposed two-phase IBC with low-cost microcontroller has been implemented in Fig. 18. The experimental setup of the converter is shown in Fig. 19. And, the experimental results are generated by using Arduino Nano microcontroller. In experimental setup, the two Arduino Nano boards are used. One board is used as the compensator and another is used as the pwm generator. The compensator generates the pwm and RC low pass filter is used to obtain the duty cycle command. The following results are obtained by using the parameters are listed in Table III. The others parameters are the same as the converter's parameters in Table I.

TABLE III

EXPERIMENTAL PARAMETERS

Parameters	Value/Type
Capacitor	470µF, 50V Electrolytic capacitor
Load	24V, 8W Lamp
MOSFET	55V, 49A, IRF Z44
Diode	800V, 3A, BY 399

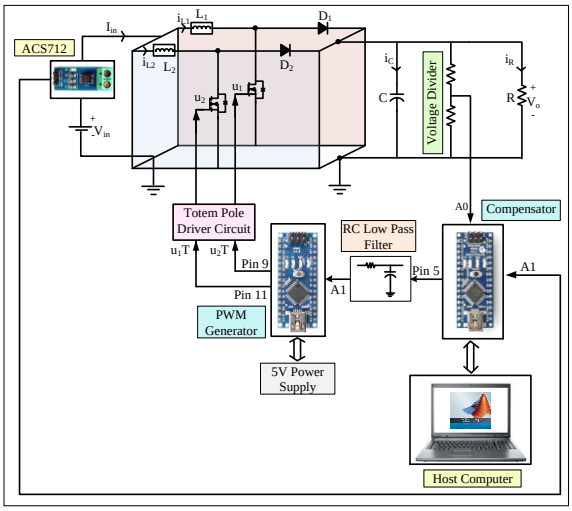


Figure. 18. Hardware setup of two-phase IBC

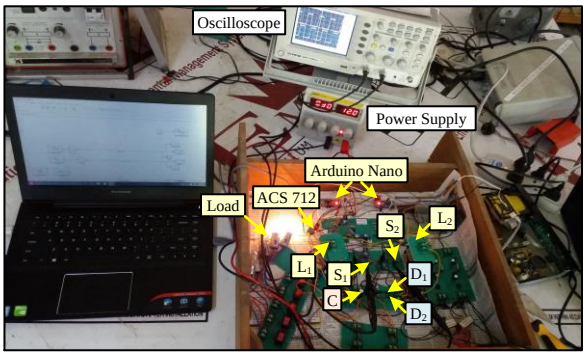


Figure. 19. Experimental setup with Arduino Nano microcontroller

Fig. 20 shows the closed loop control system using Matlab with Arduino I/O package.

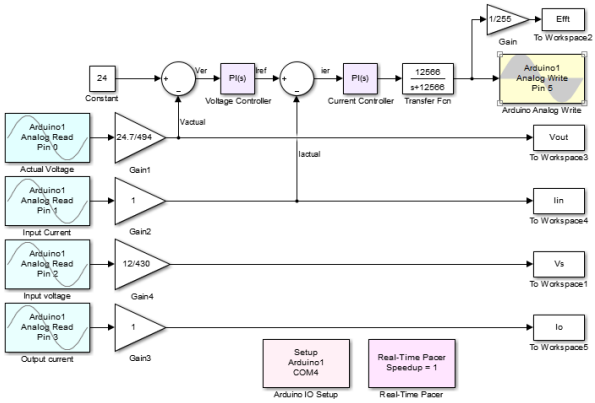
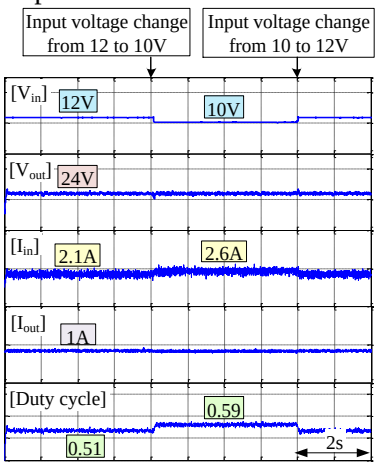


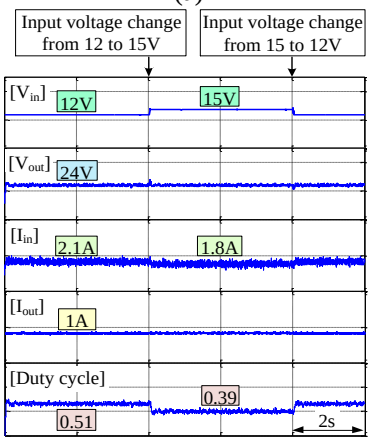
Fig. 20. Simulink model of closed-loop control with Arduino library blocks

BUPT

The experimental results are obtained by using Arduino I/O package and the sampling time is set as 2ms. Experimental transient waveforms of two-phase IBC with input voltage changes are shown in Fig. 21 for closed-loop control. Fig. 22 is presented the transient waveforms of two-phase IBC with load change in experimental.



(a)



(b)

Fig. 21. Experimental transient waveforms of two-phase IBC with input voltage change from (a) 12 to 10 to 12V and (b) 12 to 15 to 12V

The output voltage (V_{out}) response does not dramatically change when the system occurs any changes condition. The input current (I_{in}) is suddenly changed from 2.1 to 1.8A because of increasing the input voltage (V_{in}). When the input voltage is decreased, the input current is increased from 2.1 to 2.6A. Due to the increased load, the input current is varied from 2.1 to 2.75A and the output current (I_{out}) is increased from 1 to 1.33A.

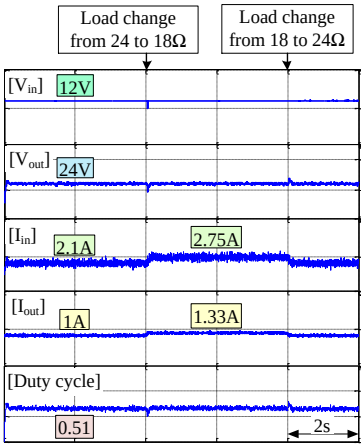


Fig. 22. Experimental transient waveforms of two-phase IBC with load change from 24 to 18 to 24Ω

It is observed that the experimental results are similar to simulation results, the output voltage is constant although the system occurs any changes condition. Therefore, the proposed converter gives satisfactory results in closed-loop system.

VI. Conclusion

This paper presents the proper PI controller design for average current mode control of two-phase IBC using bode analysis. The experimental results are presented by using low-cost Arduino Nano microcontroller to validate the simulation results. In simulation results, the output voltage response is smooth compared to experimental results because all parasitic elements include in experimental circuit. The input current and output current also have noise in experimental results because of using current sensor. It is being observed that the output voltage response for the closed-loop control of two-phase IBC during disturbances such as input voltage and load changes is satisfactory.

References

[1] Simon Ang, Alejandro Oliva, Power-Switching Converters. Second Edition, Taylor & Francis Group, 2005.

[2] Mohamed Bougrine, M.Benmiloud, A.Benalia, E.Delaleau, M.Benbouzid, "Load Estimator-based Hybrid Controller Design for Two-Interleaved Boost

BUPT

Converter dedicated to Renewable Energy and Automotive applications", ISA Trans, Vol. 66, pp. 425-236, 2016.
[3] Amar Bouafassa, Lazhar Rahmani, Saad Mekhilef, "Design and Real Time Implementation of single phase Boost Power Factor Correction Converter", ISA Trans, Vol 55, Malaysia, 2014, pp. 267-274.
[4] Subrata Banerjee, Arnab Ghosh and Niraj Rana,"Design and Fabrication of Closed Loop Two-Phase Interleaved Boost Converter with Type-III Controller," Industrial Electronics Society (IECON) 42nd Annual Conference of the IEEE, India, 2016, pp. 3331-3336.
[5] Mummadi Veerachary, Tomonobu Senjyu and Katsumi Uezato, "Modeling of closed-loop voltage-mode controlled interleaved dual boost converter," Computers and Electrical Engineering, Vol. 29, Japan, 2003, pp. 67-84.
[6] H. M. Mallikarjuna Swamy, K. P. Guruswamy and Dr. S. P. Singh, "Design and Implementation of Two Phase Interleaved DC-DC Boost Converter with Digital PID Controller," International Journal of Electrical and Electronics Engineering (IJEEE), Vol. 3, India, 2013, pp. 99-104.
[7] Fellipe S. Garcia, Jose A. Pomilio and Giorgio Spiazzi, "Modeling and Control Design of the Interleaved Double Dual Boost Converter," IEEE Trans. Ind. Electronics, Vol. 60, no. 8, pp. 3283-3290, Jun. 2012.
[8] Sandeep Kolluri and Lakshmi Narasamma N, "Analysis, Modeling, Design and Implementation of Average Current Mode Control for Interleaved Boost Converter," Power Electronics and Drive Systems, IEEE 10th International Conference, India, 2013, pp. 280-285.
[9] Hung-Chi Chen, Che-Yu Lu and Li-Ming Huang, "Decoupled Current-Balancing Control with Single-Sensor Sampling-Current Strategy for Two-phase Interleaved Boost-Type Converters," IEEE Trans., Vol. 63, no. 3, pp. 1507-1518, 2015.
[10] R. Saadi, M. Bahri, M.Y. Ayad, M.Becherif, O. Kraa and A. Aboubou,"Implementation and Dual Loop Control of Two Phases Interleaved Boost Converter for Fuel cell Applications," 3rd International Symposium on Environmental Friendly Energies and Applications (EFEA), pp. 1-7, 2014.
[11] X. Huang, T. Nergaard, J.-S. Lai, X. Xu and L. Zhu, "A DSP based controller for high-power interleaved boost converters," in Proc. IEEE Appl. Power Electron. Conf., Vol. 1, pp. 327-333, 2003.
[12] C. Suyong, S. Yujin, P. Sukin and J. Hakgeun, " Digital current sharing method for parallel interleaved dc-dc converters using input ripple voltage," IEEE Trans. Ind. Informat., Vol. 8, no. 3, pp. 536-544, 2012.
[13] Esteban Sanchis, Enrique Maset and Agustin Ferreres, "High-power Battery Discharge Regulator for Space Applications," IEEE Trans. Ind. Electronics, Vol. 57, no.12, Spain, Dec. 2010, pp. 3935-3943.
[14] M. T. Tsai, D. Y. Chen, C. J. Chen, C. H. Chiu and W. H. Chang, "Modeling and design of current balancing control in voltage-mode multiphase interleaved voltage regulators," in Proc. IEEE Int. Power Electron. Conf . (IPEC), pp. 881-887, 2010.
[15] K.-M. Ho, C.-A Yeh and Y.-S. Lai, "Novel digital-controlled transition current-mode control and duty compensation techniques for interleaved power factor corrector," IEEE Trans. Power Electron., Vol. 25, no. 12, pp. 3085-3094, 2010.
[16] Roberto Giral, Luis Martinez-Salamero, Ramon Leyva and Javier Maixe, "Sliding-Mode Control of Interleaved Boost Converter," IEEE Trans. Circuits Syst., Vol. 47, no.9, Spain, 2000, pp. 1330-1339.
[17] C.Sudhakar Babu and M.Veerachary, "Predictive Controller for Interleaved Boost Converter," International Symposium on Industrial Electronics (ISIE),Vol. 2, pp. 577-581, Jun. 2005.
[18] X. Xu, W. Liu and A. Q. Huang, "Two-phase interleaved critical mode PFC boost converter with closed loop interleaving strategy," IEEE Trans. Power Electron., Vol. 24, no. 12, pp. 3003-3013, 2009.
[19] Donny Radianto, Gamal M. Dousoky and Masahito Shoyama, "Design and Implementation of Fast PWM Boost Converter based on Low Cost Microcontroller for Photovoltaic Systems", IEEE Industrial Electronics Society, 41st Annual Conference (IECON), pp. 002324-002328, 2015.
[20] Gokhan Altintas, Mehmet Onur Gulbahce and Derya Ahmet Kocabas, "Nonideal Analysis, Design and Voltage Mode Control of a Boost Converter," Power and Electrical Engineering of Riga Technical University (RTUCON), 57th International Scientific Conference, pp. 1-6, 2016.
[21] Luca Corradini, Dragan Maksimovic, Paolo Mattavelli and Regan Zane, Digital Control of High-Frequency Switched-Mode Power Converters. First Edition, Institute of Electrical and Electronics Engineers, John Wiley & Sons, 2015.